

Influence of surrounding atmosphere on crystallization of as-quenched Fe-Ni-Zr ribbon

P. Roupcová^{1,2*}, O. Schneeweiss², P. Bezdička³, P. Petrovič⁴

¹*Institute of Materials Engineering, FME, Brno University of Technology, Technická 2, 616 69 Brno, Czech Republic*

²*Institute of Physics of Materials, Academy of Sciences of the Czech Republic, Žitkova 22, 616 62 Brno, Czech Republic*

³*Institute of Inorganic Chemistry, Academy of Sciences of the Czech Republic, 250 68 Řež u Prahy, Czech Republic*

⁴*Faculty of Science, P. J. Šafárik University, 040 66 Košice, Slovak Republic*

Received 19 January 2006, received in revised form 18 April 2006, accepted 25 April 2006

Abstract

We have investigated the influence of surrounding atmospheres on crystallization of the as-quenched Fe-Ni-Zr ribbon prepared by a melt-spinning technique. The heat treatment of samples was carried out in various atmospheres – pure hydrogen, argon and ambient (air) atmosphere – and in vacuum ($\sim 10^{-2}$ Pa). Phase compositions of as-quenched and annealed states were studied by X-ray powder diffraction and Mössbauer spectroscopy. Temperature dependence of magnetic moments of samples was used for determination of critical temperatures of phase transitions. Temperature dependence of electrical resistivity was applied for determining the activation energy of crystallization. Kinetics of crystallization and final phase composition strongly depends on surrounding atmospheres used during heat treatments.

Key words: as-quenched material, kinetics of crystallization, Mössbauer spectroscopy, X-ray powder diffraction

1. Introduction

The Fe-Zr based alloys are interesting as basis of materials for hydrogen storage and also due to their ability of easy production of amorphous state. The crystalline Fe₂Zr and Fe₃Zr phases exhibit the ability to remove and purify tritium in the fuel cycle of nuclear fusion reactor, to store hydrogen and to protect materials against oxidation. According to the equilibrium phase diagram, the Fe-Zr system consists of α -Fe, Fe₂Zr, FeZr₂ and FeZr₃ stable phases and Fe₃Zr(Fe₂₃Zr₆) metastable phases [1, 2]. The Fe₃Zr(Fe₂₃Zr₆) phase may be stabilized by oxygen. The Fe-rich phases, especially FeZr₂ and FeZr₃, can be recognized by combination of the Mössbauer phase analysis and X-ray diffraction. Difficulties of the phase analysis of the Fe-Zr alloys are documented in [3] where FeZr₂ phase with diamond lattice is reported in contrary to the tetragonal phase (type CuAl₂) described in [1, 2]. All of the mentioned Fe-Zr phases are able to absorb hydrogen. The storage of hydrogen is connected with disproportionation and repropor-

tion of the phases. In the material saturated by hydrogen the nonstoichiometric α -Fe, Fe₂Zr, and ZrH₂ phases were recognized [4].

Chemical compositions of as-quenched ribbons based on Fe-Zr or Fe-Zr-Ni produced by means of a melt-spinning technique are close to the eutectic concentration (~ 10 at.% Zr) [1]. Previous studies of similar materials [5] have shown that as-quenched ribbons prepared in an inert atmosphere are homogeneous, ~ 30 μ m thick with a shade of nanocrystalline phase. It was confirmed by selective area diffraction carried out in transmission electron microscopy (TEM). More detailed investigations revealed short range order fluctuations of the atomic ordering. The differential scanning calorimetry measurement has shown two steps of crystallization. The α -Fe phase crystallized in the first step followed changing the residual amorphous phase in direction to α -Fe and Fe₃Zr. The first crystallization step was confirmed by a steep increase of magnetic moment at 840 K observed in temperature dependence of magnetic moment [6]. The magnetic properties and hydrogenation of the Fe-Zr based as-

*Corresponding author: tel.: 420 532290447; fax: 420 541218657; e-mail address: roupcova@ipm.cz

-quenched ribbons were topic of several papers, e.g. [6–9]. Low-temperature measurements indicate Curie temperature (T_C) around 200 K of the materials with the chemical composition near the eutectic concentration. The second magnetic transition occurs around 70 K. The corresponding critical temperature is usually labelled as freezing temperature (T_f). This magnetic transition was described by several theories. One of them claims that the amorphous material exhibits a short-range ferromagnetic order below T_C and a complex magnetic ordering form below T_f which is described by the two-component model. The first part has the short-range aspheromagnetic order and the second part is the spin glass [7]. The other model proposes that the magnetic behaviour is superposition of three magnetic states: spontaneous magnetization causing of single-wave transition, fluctuation of local magnetization, and fluctuation of spin density [9]. The general magnetization of these components transforms in dependence on temperature and external magnetic field. The coercivity of the materials is increasing with decreasing temperature [6, 7]. An electrochemical hydrogenation causes an increase in T_C and a decrease in T_f [6, 8].

In this paper we describe the influence of surrounding atmospheres on crystallization of Fe-Zr-Ni as-quenched ribbons from the point of view of changes in kinetics of crystallization and in phase composition of crystalline state.

2. Experimental details

The as-quenched ribbons ($\text{Fe}_{90}\text{Ni}_2\text{Zr}_8$) were prepared by melt spinning technique in an inert atmosphere. The heat treatments were carried out in vacuum (10^{-2} Pa), in hydrogen (5N), argon (4N) and ambient atmosphere. The temperature dependences of magnetic moment (thermomagnetic curves) and hysteresis loops were carried out by the vibrating sample magnetometer (VSM) in the temperature range 293–1093 K in vacuum ($\sim 10^{-1}$ Pa). Electrical resistivity was measured by the four-point method. ^{57}Fe Mössbauer spectra measured using $^{57}\text{Co}/\text{Rh}$ source were carried out in the transmission geometry (MS) and in the scattering geometry using detection of conversion electrons (CEMS). MS gives information on the ribbons in their whole thickness while conversion electrons originate from a ~ 300 nm thick surface layer only. Calibration of the Mössbauer spectra was done relative to $\alpha\text{-Fe}$ at room temperature. For computer processing of the spectra, a CONFIT package was used [10] yielding the values of the relative spectrum area A and values of the hyperfine parameters including hyperfine magnetic induction B_{hf} , isomer shift δ , quadrupole splitting ΔE_Q , and quadrupole shift ε_Q [11–13]. X-ray diffraction measurements (XRD) were

performed with Siemens D5005 using $\text{CuK}\alpha$ radiation equipped with diffracted beam monochromator. Qualitative analysis was performed with Diffrac-Plus software package (Bruker AXS, Germany, version 8.0) and JCPDS PDF-2 database releases 2004. Topas, version 2.1 with structural Rietveld models based on ICSD database was used for quantitative analysis of XRD patterns.

3. Results and discussion

The chemical composition of the as-quenched ribbon was checked by conventional Energy Dispersive X-ray analysis (EDX) and it gave 84 wt.% Fe, 14 wt.% Zr, and 2 wt.% Ni. The Mössbauer phase analysis revealed 99.8 % of the amorphous (paramagnetic) phase represented by doublet with broad distribution ($\delta = -0.07$ mm/s, $\Delta E_Q = 0.2$ mm/s). A weak sextet ($A = 0.002$, $B_{\text{hf}} \sim 33$ T, $\delta = 0.0$ mm/s, and $\varepsilon_Q = 0.0$ mm/s) was ascribed to traces of the crystalline $\alpha\text{-Fe}$ phase. The CEMS spectra confirmed about 4 % of the crystalline $\alpha\text{-Fe}$ with 2% Ni on the both surfaces of the ribbon. The examples of the Mössbauer spectra are shown in Figs. 1 and 2. XRD powder diffraction revealed the mixture of an amorphous phase with a small amount of $\alpha\text{-Fe}$ with 2% Ni with the mean size of crystallites (coherent domain of diffraction) of about 9 nm [14]. More accurate determination of weight fraction of this $\alpha\text{-Fe}$ with 2% Ni phase is not possible.

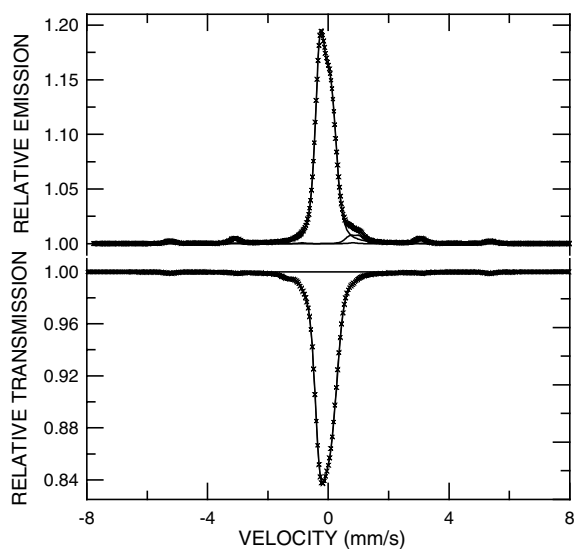


Fig. 1. Transmission Mössbauer spectrum (bottom) and conversion electron Mössbauer spectrum (top) of the as-quenched ribbon. The crosses label the experimental data and the solid curves the total fitted function. The dashed curves represent the crystalline component.

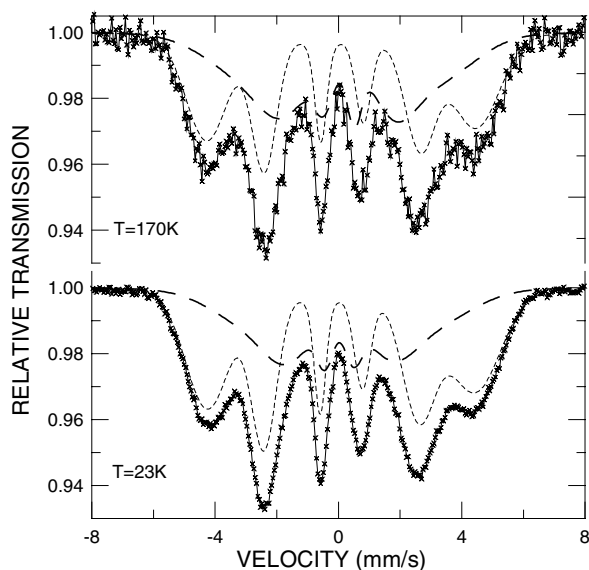


Fig. 2. Transmission Mössbauer spectra of the as-quenched ribbon taken at 170 K and at 23 K. The dashed and dotted curves correspond to the Zr-rich and Fe-rich parts of the amorphous phase, respectively.

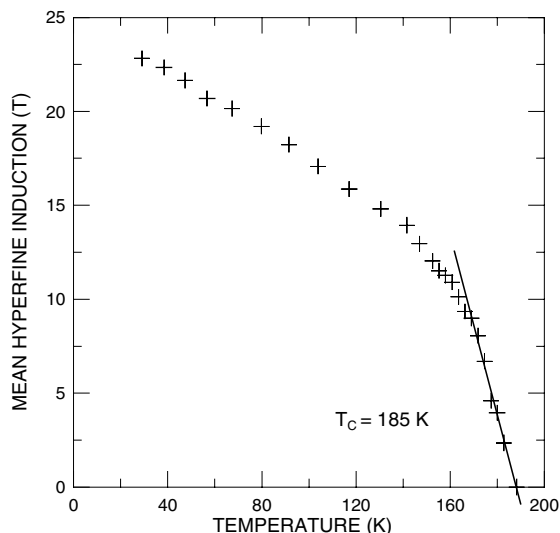


Fig. 3. The temperature dependence of hyperfine induction of the as-quenched ribbon. Determination of T_C at ~ 185 K is indicated.

Commonly used method of an internal standard could not be applied in the case of as-quenched ribbons. The T_C of the ribbon was determined by temperature scan of Mössbauer spectra down to 23 K. The data derived from the spectra are drawn in Fig. 3. From these data $T_C = 185 \pm 3$ K can be derived which is in a good agreement with the data reported in [4–7].

The thermomagnetic curve is drawn in Fig. 4. The heating part of the curve shows an increase in mag-

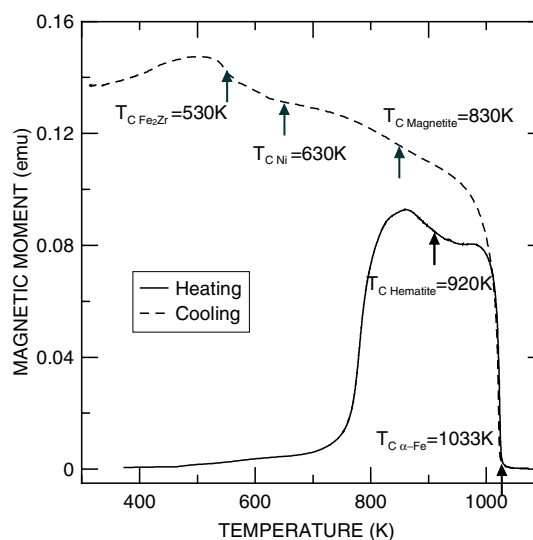


Fig. 4. The temperature dependence of magnetic moment of the as-quenched ribbon. Curie temperatures of the crystalline phases are labelled by the arrows.

netic moment at ~ 770 K corresponding to crystallization of the amorphous phase followed by decreasing steps at Curie temperatures of hematite ($T_C \sim 920$ K) and α -Fe with 2% Ni ($T_C \sim 1033$ K) [15]. On the cooling part of the curve, magnetic transition at Curie temperatures of α -Fe with 2% Ni ($T_C \sim 1033$ K), magnetite ($T_C \sim 830$ K), Ni-rich Ni-Fe ($T_C \sim 630$ K), and Fe_2Zr ($T_C \sim 530$ K) can be observed. These phases were subsequently confirmed by following Mössbauer and XRD phase analysis. The atomic fractions of Fe atoms in the phases derived from the MS spectrum were following: 0.88 in α -Fe with 2% Ni, ~ 0.10 in Fe_2Zr , ~ 0.01 in Fe_3O_4 and the remaining part (~ 0.01) in other paramagnetic phases, which cannot be distinguished unambiguously, e.g., iron atoms in Zr oxides. The α -Fe with 2% Ni solid solution is represented in MS spectrum by three sextets with $A = 0.95, 0.03, \text{ and } 0.02$, $B_{\text{hf}} = 33.0, 31.5, \text{ and } 34.0$ T, $\delta = 0.01, -0.05 \text{ and } -0.01$ mm/s, and $\varepsilon_Q = 0.01, 0.02, \text{ and } -0.01$ mm/s. Their intensities and parameters of hyperfine fields correspond well with the solid solution model for Ni content close to the nominal composition of the as-quenched ribbon (2 wt.%). From XRD data, the α -Fe with 2% Ni solid solution with particle size ~ 29 nm was determined only. The lattice parameter of the α -Fe with 2% Ni solid solution was very similar to α -Fe (2.86 nm).

The results of the measurements of temperature dependences of electrical resistivity in vacuum, hydrogen, argon are shown in Fig. 5. By interpretation of experimental data standard presumptions have been used: (i) linear growth of resistivity in dependence on temperature, (ii) sharp decrease of resistivity with start of crystallization, (iii)

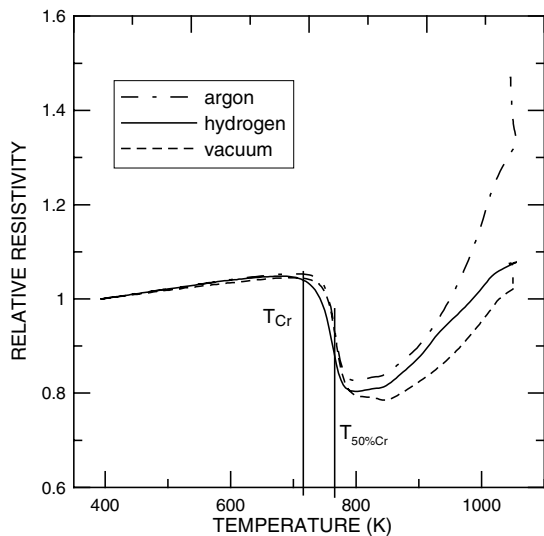


Fig. 5. Heating parts of the temperature dependences of electrical resistivity by annealing of the as-quenched ribbon in vacuum, argon and hydrogen.

Table 1. The crystallization temperatures determined from the temperature dependences of electrical resistivity

Atmosphere	Temperature (K)	
	start of crystallization T_{Cr}	50% of crystallization $T_{0.5Cr}$
ambient	678	755
argon	708	770
hydrogen	682	764
vacuum	696	768

an increase in resistivity due to formation of oxides.

A linear increase in resistivity with increasing temperature (temperature sweep $\sim 5^\circ\text{C}/\text{min}$) was observed in all applied atmospheres as well as in vacuum up to beginning of crystallization which started at ~ 700 K. In the surrounding of this temperature the resistivity increase was stopped and followed by decrease due to increase in fraction of the crystalline phase. The Mössbauer phase analysis of the sample taken from this annealing state showed that α -Fe with 2% Ni phase was formed there. The crystallization temperatures determined from the measurement of electrical resistivity are collected in Table 1. Above the crystallization temperature, electrical resistivity decreased continuously until the complete crystallization of the amorphous phase. The end of crystallization is characterized by a strong increase in resistivity. Contrary to the annealing in vacuum, hydro-

gen, argon, an ambient atmosphere annealing caused the decrease in resistivity already at a slightly lower temperature which was probably caused by nucleation and growth of oxides particles which induced crystallization of other phases. The content of oxygen in the surrounding atmosphere was the most important factor influencing the start of crystallization and its kinetics. The lowest oxygen concentration was in vacuum and hydrogen atmosphere and the increase in resistivity was less pronounced. No changes which could be ascribed to phase transitions were observed on the cooling part of the electrical resistivity curves. This difference in comparison with the thermomagnetic measurement can be explained by the dominating content of the α -Fe with 2% Ni phase in the crystalline sample, which has not another magnetic or structural phase transition below T_C . The phase composition after this heat treatment is given in Tables 2 and 3. In the sample annealed in ambient atmosphere, hematite (α - Fe_2O_3) and magnetite (Fe_3O_4) were recognized. A prevailing amount of α -Fe with 2% Ni solid solution and a lower amount of Fe_2Zr were recognized in the MS spectra of the samples after the measurement of resistivity in argon, in hydrogen, and in vacuum. Two forms of ZrO_2 besides the Fe containing phases – the stable monoclinic and the tetragonal – can be determined from the XRD measurements. The tetragonal ZrO_2 phase is metastable in pure form at room temperature and we expected that the stabilization of this phase in our samples was due to Fe ions embedded in ZrO_2 .

The isotherms of electrical resistivity at temperatures below the crystallization temperature were used for determination of activation energy of crystallization in argon and vacuum. The resistivity of annealed samples in vacuum was continuously decreasing with time. The point corresponding to the $\sim 50\%$ of crystalline phase on the isotherms was selected for the calculation of the general rate of diffusion transformation in vacuum by means of the Arrhenius equation. It was chosen as inflection point on the isotherm (S-curve). The resistivity of the sample annealed in argon was decreasing in the same way as in vacuum but after some time the resistivity started to increase due to nucleation of oxides on the surface. In this case the minimum of resistivity was chosen for the point of calculation of the general rate of diffusion transformation. Using this procedure the activation energies of crystallization in argon $Q_{Ar} = 2$ kJ and in vacuum $Q_{va} = 2.4$ kJ were derived. The lower value of activation energy in argon in comparison with the vacuum can be ascribed in higher oxygen concentration in argon and by influence of oxide formation on crystallization of the amorphous phase. The phase composition determined from MS data after the measurement of isotherms in vacuum was following: $A = 0.55, 0.05, 0.04$, and 0.36 of α -Fe with 2% Ni, Fe_2Zr , magnetite, and re-

Table 2. Phase compositions according to Mössbauer phase analysis (in atomic fraction of Fe atoms) in transmission geometry (MS) and in scattering geometry with detection of conversion electrons (CEMS)

Heat treatment	Atmosphere	α -Fe-2%Ni	Fe ₂ Zr	Fe ₃ O ₄	Fe ₂ O ₃	Amorphous phase
Annealed at 1073 K/2 hrs (MS)	ambient	–	–	0.05	0.95	–
	argon	0.89	0.02	0.06	0.03	–
	hydrogen	0.91	0.07	–	0.02	–
	vacuum	0.83	0.08	–	–	0.09
After isothermal crystallization (MS)	argon	0.79	0.08	0.04	–	0.09
	vacuum	0.55	0.05	0.04	–	0.36
Annealing at 1073 K (CEMS)	argon	0.18	–	0.77	0.05	–
	vacuum	0.96	0.03	–	0.01	–

Table 3. Phase compositions *C* (wt.%) and mean coherent length *MCL* (nm) determined from XRD

Heat treatment	Phase	Atmosphere							
		ambient		argon		hydrogen		vacuum	
		<i>C</i> (wt.%)	<i>MCL</i> (nm)	<i>C</i> (wt.%)	<i>MCL</i> (nm)	<i>C</i> (wt.%)	<i>MCL</i> (nm)	<i>C</i> (wt.%)	<i>MCL</i> (nm)
Annealed at 1073 K/2 hrs	α -Fe-2%Ni	–	–	89	80	85	55	100	25
	Fe ₃ O ₄	5	30	–	–	–	–	–	–
	Fe ₂ O ₃	75	90	–	–	5	–	–	–
	ZrO ₂ -mon.	20	30	11	30	5	30	–	–
	ZrO ₂ -tetr.	–	–	–	–	5	20	–	–
After isothermal crystallization	α -Fe-2%Ni	–	–	29	20	–	–	76	60
	Fe ₃ O ₄	–	–	45	30	–	–	–	–
	Fe ₂ O ₃	–	–	20	60	–	–	–	–
	ZrO ₂ -mon.	–	–	–	–	–	–	9	30
	ZrO ₂ -tetr.	–	–	6	20	–	–	–	–
	γ -Fe FeZr ₃	–	–	–	–	–	–	4 11	30 40

sidual oxide and amorphous phases, respectively. The samples after the measurements of isotherms in argon atmosphere consisted of $A = 0.79, 0.08, 0.04,$ and 0.09 of α -Fe – with 2% Ni, Fe₂Zr, magnetite, and residual oxide and amorphous phases, respectively.

4. Conclusion

It was shown that a surrounding atmosphere used during the crystallization heat treatment influences both kinetics and final phase compositions. Presence of oxygen caused formation of iron and zircon oxides and their amounts correspond to the oxygen concentration in the atmospheres applied during crystallization annealing. The sample crystallized in ambient atmosphere (air) was fully oxidized to hematite and ZrO₂. Besides the oxides, the contents of residual amorphous and Fe₂Zr phases changed for different atmospheres. The argon atmosphere used dur-

ing the isothermal crystallization decreased activation energy in comparison to the vacuum annealing.

Acknowledgements

This work was supported by the Czech Ministry of Education, Youth and Sports (1M6198959201) and Academy of Sciences of the Czech Republic (AV0Z20410-507).

References

- [1] OKAMOTO, H.: J. Phase Equilibria, 14, 1993, No. 5.
- [2] AUBERTIN, F.—GONSER, U.—CAMBELL, S. J.—WAGNER, H. G.: Z. Metallkde., 76, 1985, p. 237.
- [3] OTRASZ, A.: Phys Status Solidi B, 209, 1998, p. 463.
- [4] HARA, M.—HAYAKAWA, R.—KANEKO, Y. — WATANABE, K.: J. Alloys Comp., 352, 2003, p. 218.

- [5] BAKONYI, I.—MEHNER, F.—RAPP, M.—CZIRÁKI, A.—KRONMÜLLER, H.—KIRCHHEIM, R.: *Z. Metallkde.*, 86, 1995, p. 619.
- [6] BAKONYI, I.—SKUMRYEV, V.—REISSER, R.—HILSCHER, G.—VARGA, L. K.—KISS, L. F.—KRONMÜLLER, H.—KIRCHHEIM, R.: *Z. Metallkde.*, 88, 1997, p. 117.
- [7] RYAN, D. H.—COEY, J. M. D.—BATALLA, E.—ALTOUNIAN, Z.—STRÖM-OLSEN, J. O.: *Phys. Rev. B*, 35, 1987, p. 8630.
- [8] ZATROCH, M.—PETROVIČ, P.—AUBERTIN, F.—GONSER, U.: *J. Magn. Magn. Mater.*, 128, 1993, p. 365.
- [9] KAUL, S. N.—SIRUGURI, V.—CHANDRA, G.: *Phys. Rev. B*, 45, 1992, p. 12 343.
- [10] ŽÁK, T.: In: *Mössbauer Spectroscopy in Materials Science*. Eds.: Miglierini M., Petridis D. Dordrecht, Kluwer Academic Publishers 1999, p. 385.
- [11] GONSER, U.: In: *Mössbauer Spectroscopy*. Eds.: Gonser, U. Berlin, Springer-Verlag 1973, p. 21.
- [12] BOWEN, L. H.—De GRAVE, E.—VANDENBERGHE, R. E.: In: *Mössbauer Spectroscopy Applied to Magnetism and Materials Science*. Vol. 1. Eds.: Long, G. J., Grandjean, F. New York, Plenum Press 1993, p. 115.
- [13] MADDOCK, A. G.: *Mössbauer Spectroscopy, Principles and Applications*. Chichester, Horwood Publishing 1997.
- [14] COELHO, A. A.: *Topas Academic, Users Manual*, p. 31.
- [15] CORNELL, R. M.—SCHWERTMANN, U.: *The Iron Oxides. Structure, Properties, Reactions, Occurrence and Use*. Weinheim, VCH 1996.